

NUMERICAL AND EXPERIMENTAL ANALYSIS OF THE EFFECT OF VARIABLE BLADE ROW SPACING IN A SUBSONIC AXIAL TURBINE

M. Restemeier*
P. Jeschke

Institute of Jet Propulsion and Turbomachinery
RWTH Aachen University
52062 Aachen, Germany
Email: restemeier@ist.rwth-aachen.de

Y. Guendogdu
J. Gier

MTU Aero Engines,
Dachauer Strasse 665,
80955 Munich, Germany

ABSTRACT

Numerical and experimental investigations have been performed to determine the effect of a variation of the inter blade row axial gap on turbine efficiency. The geometry used in this study is the 1.5 stage axial flow turbine rig of the Institute of Jet Propulsion and Turbomachinery at RWTH Aachen University. The influence of the blade row spacing on aerodynamics has been analyzed by conducting steady and unsteady RANS simulations as well as measurements in the cold air turbine test rig of the Institute. Both potential and viscous flow interactions including secondary flow were investigated. The results show an aerodynamic improvement of efficiency and favorable spatial distribution of secondary kinetic energy by reduction of the axial gap. It is shown that this relation tends to become less pronounced for multistage turbines.

INTRODUCTION

The designer of modern turbines used in aero engines and stationary applications has to accommodate a variety of constraints and degrees of freedom to obtain an optimal geometry for a given set of requirements. The axial spacing between the blade rows is one of the parameters which could lead to shorter and lighter designs as well as impact on aerodynamic efficiency. In a real turbine application there are undoubtedly a number of additional constraints which prevent the free determination of the axial spacing. Unsteady aerodynamic forces normally limitate the

designer. Other effects of reduced significance are clearances to enable axial thermal expansion or space to integrate blade platform cooling, to name just two. The main goal of the present study is to clarify the effect of axial blade row spacing solely from the aerodynamic perspective. There have been several investigations of this topic in the past which give a contradictory picture of the situation.

A drawback of this study and most of the simple models is the neglect of shocks appearing in transsonic turbines. Results suggest the need to differentiate between subsonic and transsonic turbines while determining the optimal axial gap. All published studies to the authors knowledge claim an improvement of efficiency for larger axial gaps in transsonic turbine stages [1–4]. For subsonic turbine stages there are several effects mentioned in previous studies which can be summarized as follows.

The main idea of Smith [5] is the so-called wake effect which describes the variation of mixing losses when a wake is accelerated or diffused isentropically prior to mixing. There are several problems in assigning this effect to real-world turbines. First is the determination of the acceleration ratio for a wake deformed in a highly loaded blade passage. Second is the presence of three dimensional flows owed to the end walls leading to the formation of streamwise orientated secondary flow which strongly influence efficiency. Thirdly there have been observed strong unsteady interactions between the blade rows which are not included in this simple model.

In line with the wake-effect Praisner et al. [6] showed that stretching of wakes in a subsequent turbine blade row should

*Address all correspondence to this author.

augment losses in contrast to undisturbed mixing. According to these findings larger axial gaps should be advantageous if end wall friction is neglected. The opposite is claimed by Rose and Harvey [7] who showed that for the ideal case of complete distinction between wake and freestream fluid the work extraction in the turbine reduces mixing losses in contrast to undisturbed out-mixing. This should give smaller axial gaps an advantage.

Recent studies tend to cover the full three-dimensional flow field and all of them find a smaller axial gap advantageous. Park et al. [8], Kikuchi et al. [9], Yamada et al. [10] and Gaetani et al. [11–13] investigated subsonic turbines with an aspect ratio of 1.1 to 2 and reported a 1-2% efficiency gain for the smallest axial spacing relative to the largest. They identified a periodic interaction between stator secondary flows and the formation of the rotor passage vortex mainly observed in the hub region although Kikuchi [9] and Yamada [10] investigated a shrouded rotor.

Older studies by Cizmas [14] and Van de Wall et al. [15] show a different behavior. The smallest axial spacing does not lead to the highest efficiency. However there is no obvious explanation for all these different findings. One may be the general existence of an optimal axial spacing close to zero which may or may not be covered in former studies. This is the motivation for the current study. It is intended to increase the knowledge in this field of turbine aerodynamics. Off-design investigations are also planned to elaborate the influence of blade loading and incidence angle on the correlations found.

EXPERIMENTAL SETUP

Test Rig

The present research was conducted at the axial cold air turbine test rig of the Institute of Jet Propulsion and Turbomachinery at RWTH Aachen University, shown in Fig. 1. Due to the fact that most of the former studies deal with single turbine stages but in most applications multistage turbines are used a 1.5-stage configuration was investigated. It consisted of a rotor framed by two stator rows. This offered the possibility of investigating the additional influence of upstream flow on the stator of the next stage. The test rig featured modern 3D-blading similar to a typical LPT turbine, although the aspect ratio is relatively low and similar to that of HPT turbines. It resembled a compromise between reasonable chord lengths and a mass flow limitation of the air supply system. The Zweifel numbers of the blade rows were optimized for high efficiency [16]. The turbine operated at a design rotor speed of 3500 rpm and a total pressure ratio of approx. 1.3 at 1.66 bar inlet total pressure. The combination of higher pressure and fairly low temperature led to Reynolds numbers in the Range of $3.3 - 8.1 \cdot 10^5$ based on chord length and bladerow exit conditions. This resembles conditions at take-off of a typical middle stage of an LP-turbine according to Halstead et al. [17]. Bypass transition was likely to be the dominant effect on the blade suction surfaces. The mass flow rate under design conditions was

TABLE 1: TURBINE DESIGN PARAMETERS

	Stator 1	Rotor	Stator 2
Number of Blades [-]	33	44	66
Tip Diameter [mm]	600.0	600.0	600.0
Hub Diameter [mm]	490.0	490.0	490.0
pitch-chord ratio t/l [-]	0.9	0.98	0.71
aspect-ratio h/l [-]	0.95	1.4	1.51
projected aspect-ratio h/l_{ax} [-]	1.45	1.77	1.57
Zweifel number [-]	0.79	0.95	0.89
Reynolds number [-]	$8.1 \cdot 10^5$	$5.2 \cdot 10^5$	$3.3 \cdot 10^5$
Radial Tip Clearance [mm]	-	0.3	-
Aver. Inlet Angle [°]	90.0	46.5	137.6
Aver. Exit Angle [°]	19.9	159.6.0	30.8

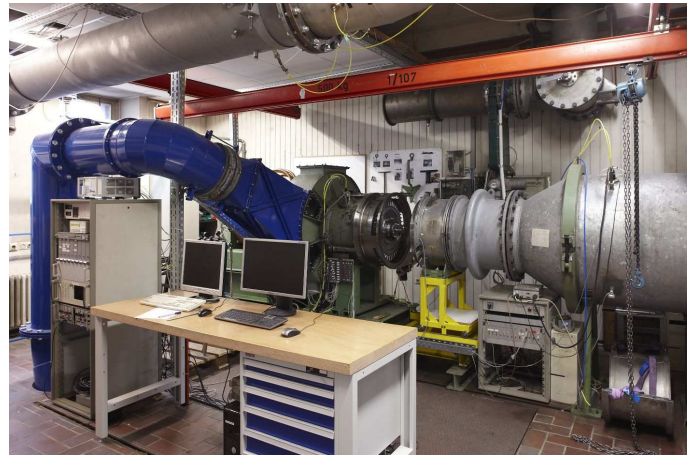


FIGURE 1: SIDEVIEW OF TURBINE TEST RIG

8.1 kg/s and was measured by a calibrated venturi meter. Overall parameters of the configuration used are given in Tab. 1.

The test rig featured a microcontroller-based operating point regulator insuring stable inlet and outlet pressure levels as well as a constant rotor speed during the measurements. This was realized by application of quick reacting bypass valve actuators at inlet and outlet as well as a controllable eddy current brake.

TABLE 2: INVESTIGATED INTER-BLADE ROW GAPS

	Gap A	Gap B	Gap C
δ	8mm	19mm	30mm
$\delta/l_{ax,Le1}$	0.21	0.50	0.79
$\delta/l_{ax,Le2}$	0.22	0.54	0.85



FIGURE 3: PROBES USED FOR THE TRAVERSE PLANE INVESTIGATIONS

Data Acquisition

Time mean measurements were performed in all axial measurement planes one to three using five-hole probes with internal thermocouple as well as 360° rake measurements at turbine exit. The instrumentation at MP4 consisted of six rakes with three radial total pressure taps each. These rakes were mounted on a circumferentially traversable ring located at measurement plane four. By traversing the ring at an angle of 70° in steps of 0.25° six overlapping chunks of measurements captured possible circumferential asymmetry in the outlet plane which is important for proper detection of small differences in efficiency. The efficiency was then calculated by the following equation under usage of rotor torque and mass flow.

$$\eta_t = \frac{N \cdot D \cdot \pi}{30 \cdot \dot{m} \cdot c_p \cdot T_{t1} \left(1 - \left(\frac{p_{t4}}{p_{t1}} \right)^{\frac{\kappa-1}{\kappa}} \right)} \quad (1)$$

The unsteady measurements were conducted with probes featuring internal semiconductor pressure transducers and hot wire anemometry for the examination of the detailed flow field behind the blade rows. The random fluctuating part of the signal was used as a measurement of turbulence in the flow field. All used probes are shown in Fig. 3. The probes were traversed by a mechanism driven by stepping motors adapted to movable casing rings. The measurement grid consisted of 41 radial and 23 pitch-wise measurement locations which led to 943 points for one field, as shown in Fig. 4. The measurement grid covered one pitch of the first stator while the maximum number of points was limited mainly by the measurement time for one day of operation. A local grid refinement was used in the endwall region for higher resolution of secondary flow patterns. All unsteady measurements were recorded by a multi channel analog digital converter pc card which operated with a sampling rate of 250kHz and 16bit resolution. This insured sufficient accuracy in time and signal resolution. A phase-locked ensemble average [18] was performed on the derived physical properties to separate the deterministic

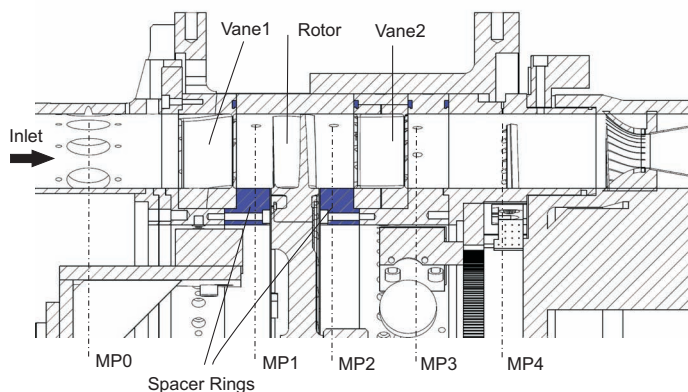


FIGURE 2: MEASUREMENT PLANES AND BLADING

Axial Gap Configurations and Measurement Planes

The test rig featured some unique properties to allow easy modification of axial spacing. The channel height is held constant throughout the machine. Furthermore the rotor is supported one sided whereas both stator rows are movable in the axial direction. Spacer rings between the stators and the rotor were used to adjust the hub-sided cavities. The blade row spacing between both first vane and rotor as well as rotor and second vane was varied symmetrically. Other configurations were possible but were not applied owed to the time and effort required. To insure comparability of the different geometric settings the clocking effect was compensated by circumferential movement of the second stator while the axial gap was changed. The three different spacings of this study are given in Tab. 2.

Fig. 2 shows a sectional drawing of the bladed section including measurement plane positions. The inlet plane is named zero and is located two axial chord lengths in front of the first stator. Probe traverse planes are located behind every blade row and consecutively named one to three. Plane four contains probe rakes for efficiency measurements which are described in detail in the following section.

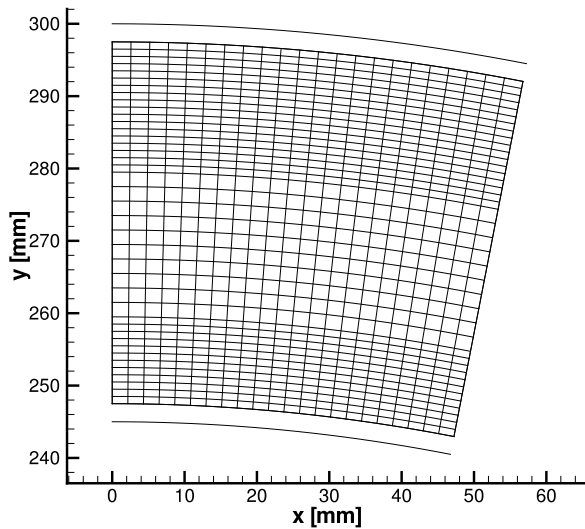


FIGURE 4: MEASUREMENT GRID IN S3 PLANE

and the random parts of the signals. Pre-examinations showed that 232 sampled rotations per measurement location were sufficient. All data was stored as raw data as well to preserve the information of the original measurement.

Measurement Uncertainty

The experimental results that were compared with numerical values and the efficiency data are afflicted with measurement errors whose magnitude has to be known. The error of the probe traverse plane measurements in the test rig is below 0.2° for the flow angles α and γ , 0.001 for Ma , 40.2 Pa for pressures and 0.3 K for T_t . Further information on uncertainty of the steady measurements can be found in Poehler et al. [19].

Concerning the time-resolved measurements Walraevens [20] calculated a measurement uncertainty of 0.5% of the measured value. For all efficiency measurements knowledge of the correct massflow and rotor torque is crucial. For this reason both the torque meter and the venturi meter including pressure transducers were extensively calibrated. The overall yielded error of efficiency was 0.23% whereas the repeat accuracy between two days of measurement was below 0.08% when the same assembly was retained. Measurement accuracy for massflow and torque were 0.15% and 0.1% respectively.

Indexing of stators one and two was another possible source of error in investigating axial gap effects. The vane numbers are 33 and 66 respectively which resembled a half clockable configuration. Peak efficiency clocking position was determined and used throughout this investigation. To maintain peak efficiency for all experiments the second stator had to be moved to the same

relative position of the stator one wake trajectory relative to the leading edge of stator two. This was also valid for the numerics. Interestingly, we concluded, that the relative positions of the two stators contributed very little to the overall losses. The values were considerably below measurement accuracy for the nominal gap B.

NUMERICAL SCHEME

Description of the Flow Solver

For all simulations the solver TRACE (Turbo Machinery Research Aerodynamic Computational Environment) in version 6.7 was used. This is a Reynolds-averaged Navier-Stokes solver based on a cell-centered finite volume approach and was developed at the Institute of Propulsion Technology in cooperation with MTU Aero Engines. For turbulence closure a two-equation $k - \omega$ model was used. The theory and methods of TRACE as well as code validation on the basis of experimental results can be found in [21], [22]. A standard MUSCL approach in combination with a Roe upwind-based convective flux-difference splitting and a central discretization of viscous terms provided second-order space accuracy. Time integration was performed via an implicit dual-time stepping three step backward euler algorithm insuring second-order accuracy in time as well. The solver was parallelized based on domain decomposition using MPI communication library, and therefore it can be run on a wide variety of distributed or shared memory computer systems. In the present work all computations were carried out on the cluster of the RWTH Aachen consisting of infiniband coupled nodes running under an X86-64 Linux architecture.

Computational Grid

The grid was generated with G3DMESH by CFD Norway [23], which provides automated template based structured grid meshing. Owing to the expected variation in mesh quality in the trailing edge region when meshing very small axial blade row spacings an unusual approach was used. The mesh for all three blade rows remained the same for every axial spacing whereas the emerging space in between was filled with equidistant blocks without sheared cells. Figure 5 gives an overview of the complete domain for the steady calculations. The blade/vane count in this setup offered the possibility to model an eleventh fraction of the whole annulus of the turbine which avoids domain scaling or phase-lagged unsteady computations. The spatial resolution was reasonably high to resolve the convection of wakes in downstream passages. In the rotor passage the resolution was 166 points streamwise and 119 points pitchwise. All rows contained 65 grid points in spanwise direction owing to the application of wallfunction on hub and tip with $y^+ \approx 30$. In contrast $y^+ \approx 1$ was insured on all blade surfaces for the low Reynolds approach. In summary the unsteady grid contained over 17 million nodes in

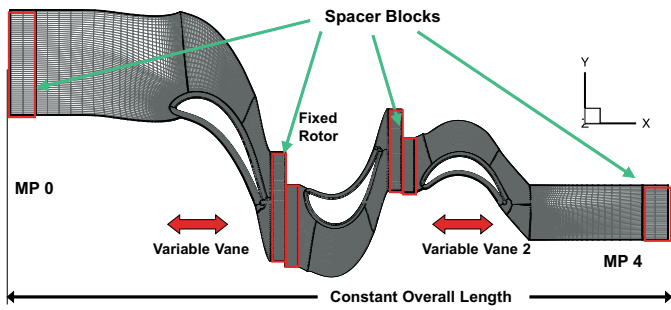


FIGURE 5: COMPUTATIONAL DOMAIN FOR ONE PASSAGE PER BLADE ROW AT MIDSPAN

13 passages which limited the excessive use of parameter variations due to available cpu power. Parallelization was enabled by assigning the 174 blocks to several cpus. A reasonable number of cpus is 32 for this case as a trade-off between the computation and communication time of the processes.

Boundary Conditions

Non-reflecting boundary conditions [24] were applied at the inlet and outlet plane. In order to couple moving and stationary blade rows and to combine non-matching block boundaries inside the domain a fully zonal approach is available [25]. The inlet boundary condition values were chosen to resemble the experimental setup as much as possible. A radial distribution of measured values was provided at the inlet. It contained total pressure and temperature as well as flow angles and turbulence properties measured by hotwire anemometry. Figure 6 shows the radial inflow Mach number profile and turbulence intensity for several subsequent measurements. It is illustrated that the variance of the values was very low. At the outlet of the domain static pressure at midspan and a radial equilibrium were prescribed. This is a reasonable presumption because of the large distance between trailing edge of the second stator and the outlet plane. The application of the implemented multi-mode transition model [26] to the blade walls was considered to be necessary to capture the wake-induced boundary layer transition on the downstream rows. After preliminary unsteady 2D-simulations of the present geometry showed very little effect on the $\Delta\eta$ results while increasing the numerical cost by an order of magnitude, however, it was decided to switch to fully turbulent simulations. Increase in computational cost was essentially caused by the smaller required time step size of the multi-mode transition model. Therefore transition related losses were not covered by the numerics in this investigation.

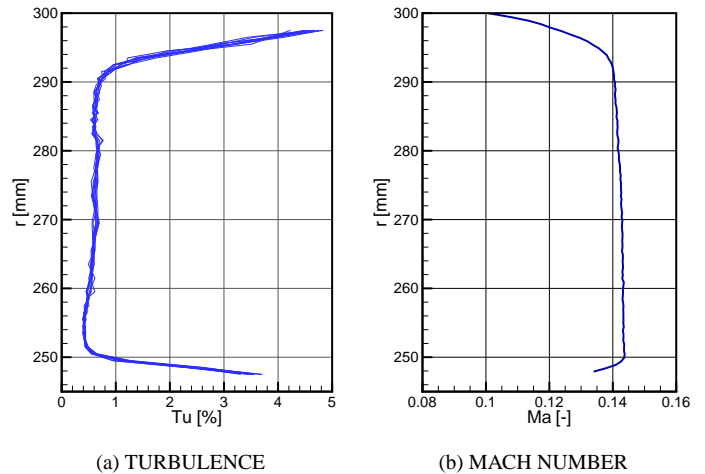


FIGURE 6: RADIAL DISTRIBUTION OF MEASURED IN-FLOW PROFILE

Unsteady Setup and Convergence

The calculations were carried out using 256 time steps per period which corresponds to roughly 42 time steps per stator two period. To determine the computational error the solution was compared with another one using 512 time steps per period. No significant difference in the flow field or efficiency could be found. The dual time stepping approach was conducted by computing 25 inner iterations per physical time step which was sufficient to reduce the residual of the equation system. Convergence of all unsteady simulations was ensured by application of the method described by Clark and Grover [27]. Starting from a converged steady state calculation 12 to 15 simulated periods were necessary to meet the convergence criteria.

RESULTS

Overall Aerodynamic Performance

The overall performance of the turbine configuration was calculated by massflow weighted average values of total temperature and total pressure near the inlet and outlet of the domain. The axial positions of the averaging planes matched the experimental ones. The resulting total to total isentropic efficiency for gaps A to C is shown in Fig. 7. The unsteady simulation shows that the smaller axial spacing leads to an efficiency improvement of 0.2% compared with the nominal spacing B while further increase of axial spacing leads to disproportionately low efficiency. It is also clearly shown that the unsteady calculations tend to provide better agreement with the experimental data. In general the offset between numerics and experiments is due to the fully turbulent simulation of the boundary layer on all blade walls whereas in the experiments partly laminar regions were ob-

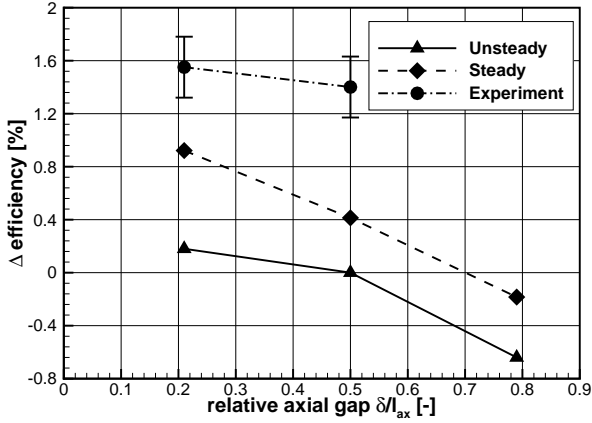


FIGURE 7: CFD PREDICTED OVERALL PERFORMANCE

served. Time and massflow averaged entropy s/R (Eqn. 2) can be used to show where the losses occur and is defined as follows. This is based on the reasonable assumption of adiabatic flow with negligible heat transfer through the control volume boundary.

$$s/R = \frac{\kappa}{\kappa - 1} \ln(T) - \ln(p) \quad (2)$$

Figure 8 shows the value of entropy plotted against the axial coordinate. Since the entropy is a nonlinear function of static pressure p and static temperature T a slight error occurs when time averaging precedes spatial averaging. This occurs in regions of high temporal variation. However the overall magnitude is still valid. The main difference between all three axial spacings was observed between start of the rotor passage and ends behind the second stator whereas the magnitude of entropy at the trailing edge of the first stator remains unchanged. If the total pressure loss coefficient ζ (Eqn. 4) is evaluated instead of s/R a slight increase could be observed for the trailing edge of the first stator and the small spacing which is caused by the upstream work extraction process of the rotor. All this leads to the assumption that variations in rotor and second stator flow field are mainly responsible for the variation of losses. To elaborate on this assumption more detailed data of these two blade rows are investigated in the following sections.

Rotor Flow Field

The three-dimensional flow field inside the rotor passage is dominated by the periodic cutting of the first stator wake and interaction of the stator secondary flow with the rotor passage vortex. In the tip region the strong tip clearance vortex of the unshrouded blade dominates the flow field [19]. This is the reason why the periodic suppression of the rotor passage vortex is

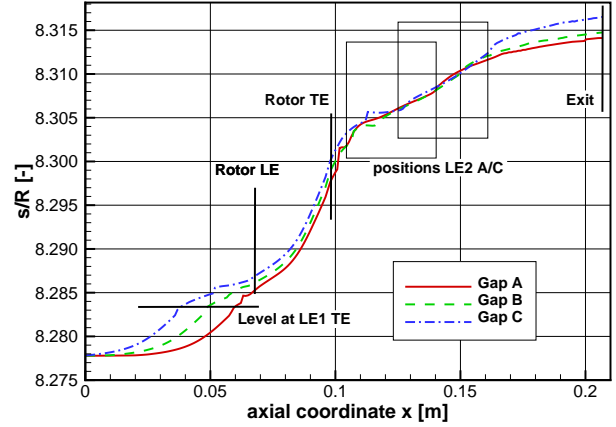


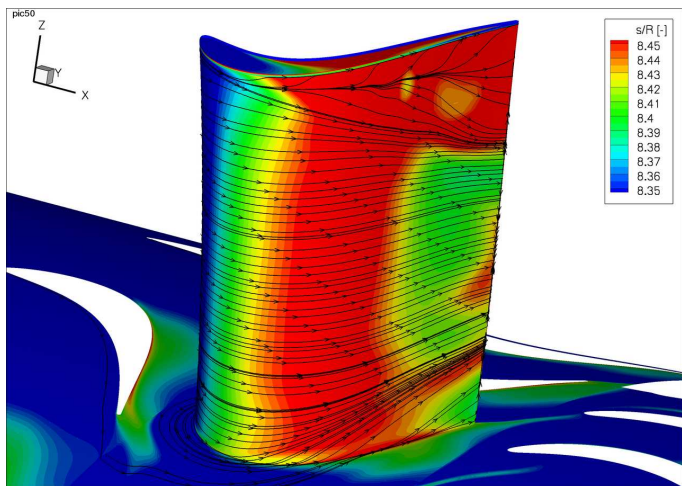
FIGURE 8: AXIAL GROWTH OF LOSSES OVER ENTIRE TURBINE

extremely weak in the tip region. Figure 9 shows the streamlines on the rotor suction side for gaps A and C for the time instant of maximum extent of the passage vortex. It can be seen that the nearly two dimensional freestream region around midspan is reduced from almost 50% to 30% span for the larger axial gap. The reduced frequency Ω , defined as the blade passing frequency times the distance from leading to trailing edge divided by the average axial free-stream velocity through the blade passage, is 0.76 for the rotor and 1.12 for the second stator. Ω characterizes the level of unsteadiness as described by Greitzer [28].

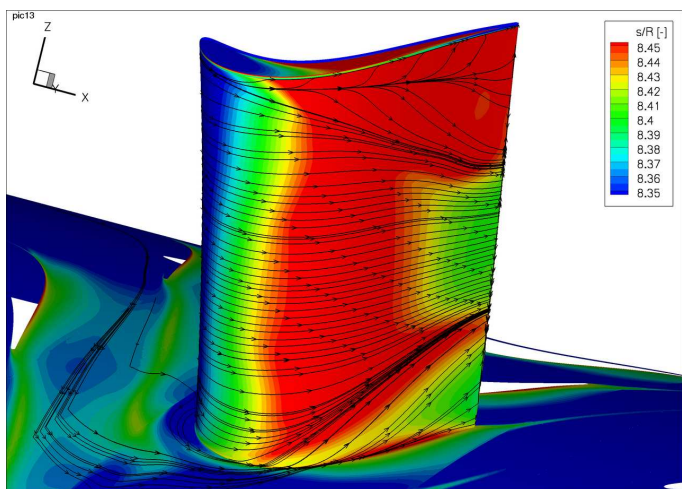
$$\Omega = \frac{f_P \cdot l_{ax}}{c_{ax}} \quad (3)$$

This means the unsteadiness related to the convection through the passage is at a low level, typical for rotors in highly loaded turbine stages and higher for the second vane. Figure 9 is colored with the dimensionless entropy s/R to identify the streamwise position of the stator wake in the rotor passage. When time-averaged results are compared the difference in passage vortex size between the small axial gap and the largest one is still evident but less significant. It is difficult to determine the proportion of the unsteady periodic effects relative to the natural growth of the side wall boundary layer in the axial space between the blade rows. However, comparing time-averaged results with a steady state solution show clearly the periodic variation of the passage vortex size is stronger in the large gap case and therefore expectedly higher losses occur.

$$\zeta = \frac{\overline{p_{t0}} - \overline{p_{t1}}}{\overline{p_{t1}} - \overline{p_1}} \quad (4)$$



(a) GAP A



(b) GAP C

FIGURE 9: STREAMLINES ON ROTORBLADE COLORED BY ENTROPY s/R

The flux averaged total pressure loss coefficient, defined according to equation 4, is given in table 3. The total pressure loss coefficient reveals the same trend as seen in the entropy plot except the axial development. All these results are in line with previous studies on similar turbine configurations by Yamada et al. [10] and Gaetani et al. [11].

Second Stator Flow Field

In comparison with the rotor flow field the second stator is periodically affected by both the rotor wake and its secondary flows as well as the still existing secondary flows produced by the first stator row. The difference between them is the strength and the sense of rotation of corresponding incoming secondary

TABLE 3: TOTAL PRESSURE LOSS COEFFICIENT

	Gap A	Gap B	Gap C
Vane 1	0.0499	0.0517	0.0548
Rotor	0.1168	0.1251	0.1349
Vane 2	0.1125	0.1183	0.1181

vortices. In the tip region the rotor tip leakage vortex is still dominating. One important feature of the present turbine rig is the blade number between the first and the second stator, which is 33 to 66 and leads to two alternating flow fields in front of adjacent second stator vanes. While the rotor wake is uniformly distributed one stator two "sees" patterns of the first stator wake whereas the other one does not. By comparing the two second

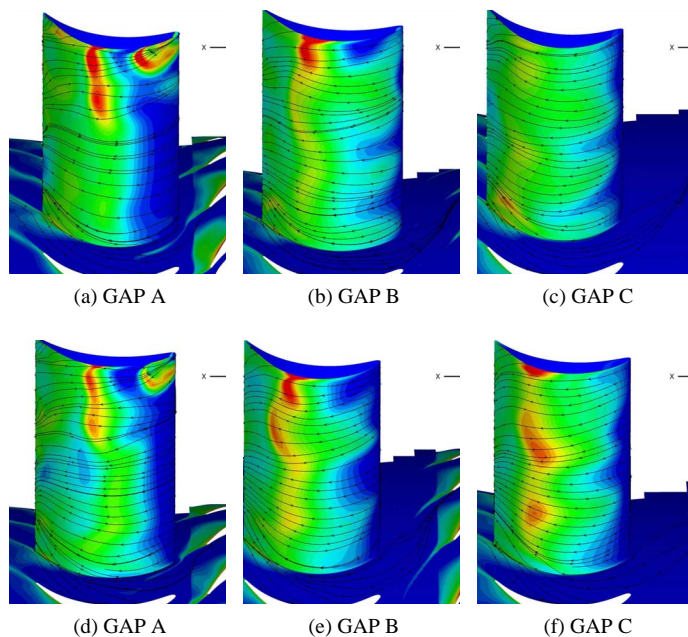


FIGURE 10: SECOND STATOR SUCTION SIDE STREAMLINES: (a)-(c) WITHOUT FIRST STATOR WAKE, (d)-(f) INFLUENCED BY FIRST STATOR WAKE

stator vane passages we have an opportunity to gather information on the influence of the first stator wake/vortex system on the second stator. The clocking position remains constant for all axial spacings as mentioned in the section: measurement uncertainty. Figures 10 (a)-(c) show the suction side of the non affected passage whereas Fig. 10 (d)-(f) illustrate the flow influenced by the first vane. All figures are taken at the time instant

of maximum strength of the passage vortex in the second vane similar to Fig. 9 for the rotor. Neither in the hub region nor in the tip region a significant influence of the stator one secondary flows on the passage vortex size can be observed. For further investigation of secondary flows the streamwise vorticity is used as a measurement quantity as proposed by Horlock and Lakshminarayana [29] although the limitations of this definition are known, see Persico et al. [30]. The vorticity of the viscous velocity field is calculated as follows.

$$\vec{\omega} = \begin{pmatrix} \omega_x \\ \omega_y \\ \omega_z \end{pmatrix} = \frac{1}{2} \begin{pmatrix} \frac{dw}{dy} - \frac{dv}{dz} \\ \frac{dz}{dx} - \frac{dx}{dz} \\ \frac{dv}{dx} - \frac{du}{dy} \end{pmatrix} \quad (5)$$

Streamwise vorticity ω_{sw} is then derived by projecting the local vorticity on the local velocity vector.

$$\omega_{sw} = \frac{1}{|\vec{c}|} (\omega_x u + \omega_y v + \omega_z w) \quad (6)$$

In Figure 11 the comparison of circumferentially and time averaged streamwise vorticity between the adjacent second stator vanes and a steady-state computation is shown. We observed a difference between the two passages and between the axial spacings. For the large axial gap C there is an amplification of streamwise vorticity near the hub and tip in the passage which is mainly affected by first stator secondary flow patterns. This is identified as the passage vortex of the second vane. For the non-affected passage which is mainly governed by rotor secondary flow field a reduction of the same quantity can be discovered. It shows a negative effect of stator one to stator two.

For the small axial spacing A the picture is more difficult. Both passages reveal a reduction of streamwise vorticity near the hub and tip region comparing to the steady state solution. This can be explained by the stronger influence of the rotor in both passages. Although it is not clear which mechanism amplifies the streamwise vorticity in the midspanregion for the small axial spacing A.

The results indicate that the first vane secondary flow patterns have an amplifying effect on the secondary flow in the second vane passage. This is contradictory to its effect on the rotor passage which has in turn a damping effect on the secondary flow in the second vane passage

EXPERIMENTAL RESULTS

To investigate the overall performance of the turbine rig with respect to the axial spacing an operating map was recorded which is provided in Fig. 12. Two axial spacings were evaluated for efficiency but the larger, gap C, had problems with the rake measurements and is omitted here. The smaller axial spacing A leads

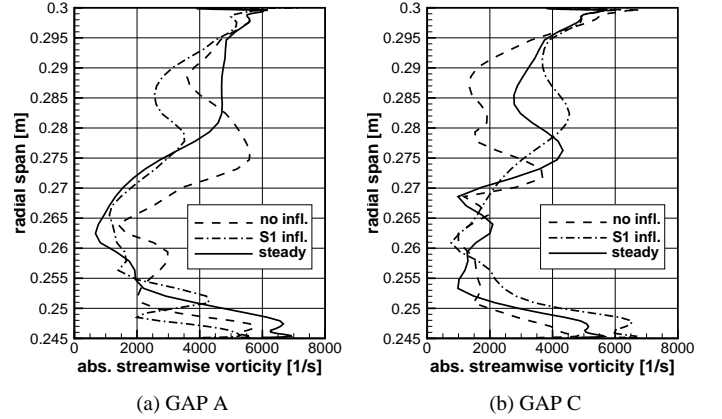


FIGURE 11: RADIAL DISTRIBUTION OF MASS AVERAGED ABSOLUTE STREAMWISE VORTICITY BEHIND THE SECOND STATOR

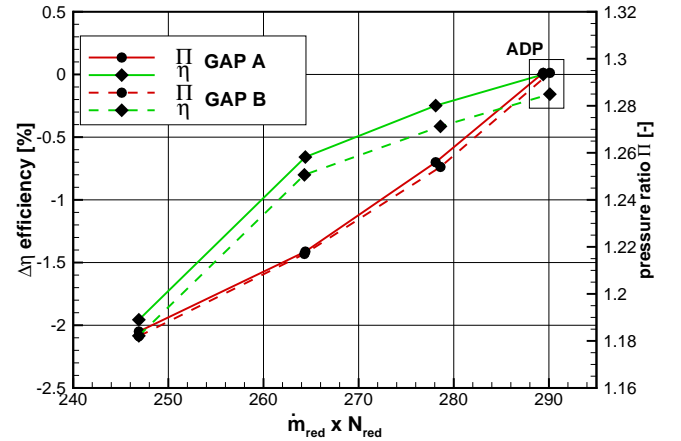


FIGURE 12: MEASURED TURBINE OPERATING MAP

to a slightly higher efficiency of 0.2% at design conditions. The difference between the two axial gaps in isentropic efficiency is very close to the numerical results shown before when we consider the measurement accuracy and modeling errors. Furthermore the plotted operating map seems plausible for the presented measurements. A further observation can be made concerning the blade incidence. Yamada [10] showed that increasing rotor incidence leads to higher efficiency gains for smaller axial gaps. Here a decrease in pressure ratio and therefore a negative incidence to the rotor leads to a lower efficiency gain for the same gap. This is also in line with the observation that the interaction between the secondary flows reduces losses in the subsequent passage.

Figure 13 shows an instantaneous snapshot of the absolute ve-

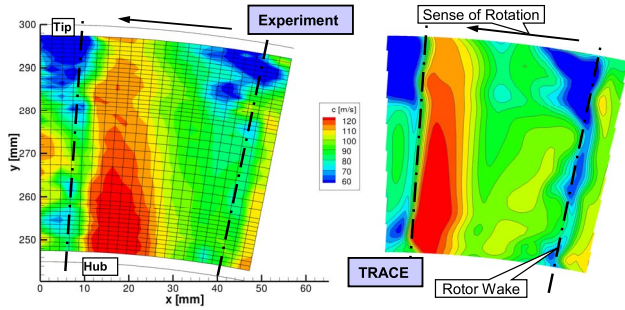


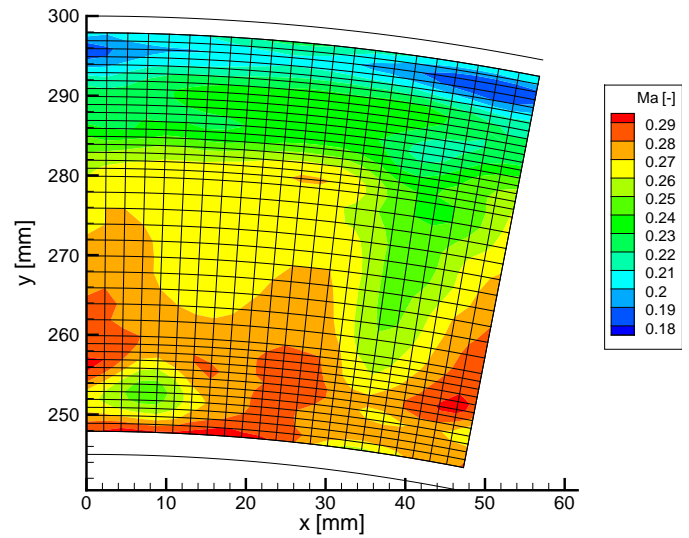
FIGURE 13: COMPARISON OF CFD AND EXPERIMENTAL DATA

locity downstream of the rotor obtained by a hotwire probe. The left dataset shows the experimental data and corresponding CFD results are shown on the right side. In general a good agreement between CFD and measurements could be obtained. This is mainly due to the adaptation of the CFD setup to the experimental boundary conditions. In Fig. 14 two measured time averaged mach number distributions behind the rotor are compared. Although the time dependent information has been eliminated it can be seen that the regions of higher mach numbers are shifted into the midspan region for the large spacing. This corresponds to the numerical data downstream of the rotor. In general the distribution in the circumferential direction is much more uniform for the large spacing than what was expected due to the first stator wake mixing. Figure 15 shows a comparison of the flow field behind the second vane for the two different spacings A and C. The level of turbulent velocity fluctuations measured by a 3D hotwire probe is shown. The overall level of turbulence is significantly lower for the larger axial spacing due to out mixing processes. For the smaller spacing a similar observation as for the CFD results can be made. The local maxima of turbulence are shifted slightly more into the midspan region but the difference between the two passages is bigger in the small axial gap case.

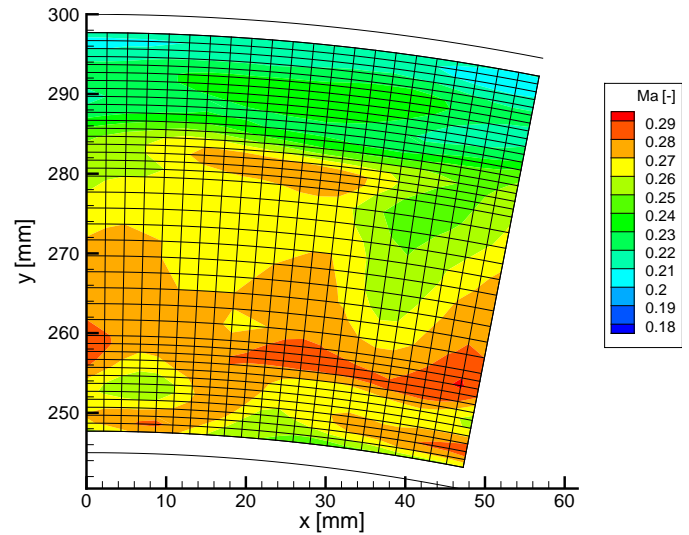
2D NUMERICAL RESULTS

Recent results point out that there are different effects which influence efficiency in a contradictory way. Wake decay in the subsequent blade row may increase or decrease losses. Decay of secondary vortices which are orientated mainly streamwise should show a different behaviour during stretching [31]. Unsteadyness caused by potential flow interaction and the negative jet effect should augment losses. Interaction between upstream secondary flows and passage vortices in the three-dimensional case influences losses as shown in this study.

A promising way to differentiate between 3D endwall effects and 2D wake/blade interaction is to compare two-dimensional simulations of the same blading at midspan with



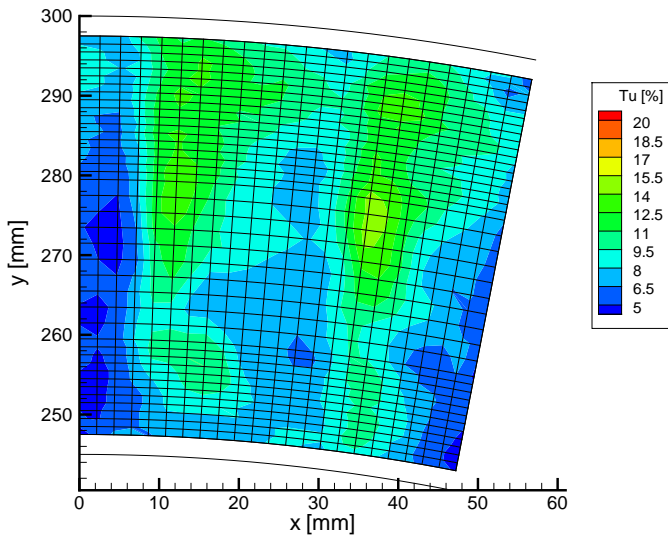
(a) GAP B



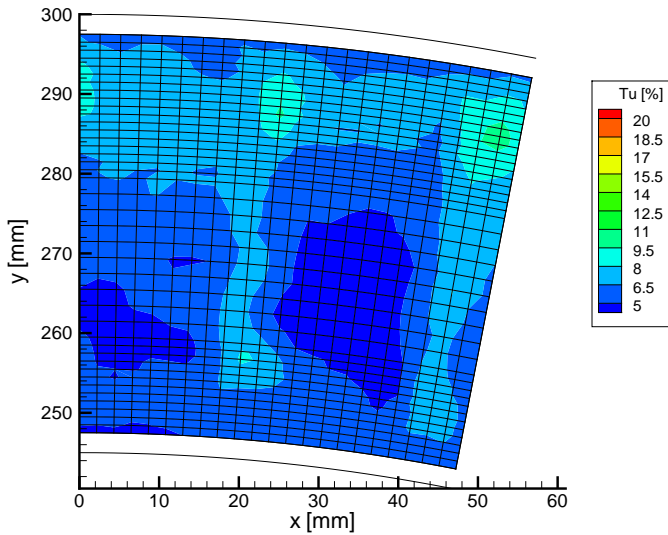
(b) GAP C

FIGURE 14: TIME AVERAGED MACH NUMBER DOWNSTREAM THE ROTOR

three-dimensional simulations. Whereas the same boundary conditions at inlet and exit were applied the results of the simulations show a different efficiency with respect to the blade row spacing from that of the three-dimensional case. The simulation results shown in Fig. 16 indicate a maximum aerodynamic efficiency for an axial gap of about 50% chord length of the stator and both



(a) GAP A



(b) GAP C

FIGURE 15: RMS TURBULENCE DOWNSTREAM THE SECOND STATOR

smaller as well as larger axial gaps tend to give lower values. Von Hoyningen-Huene [32] performed comparable simulations of the first stage of a Siemens gas turbine and obtained similar results. The detected maximum efficiency indicates there is a trade-off between wake mixing loss and loss due to unsteady fluctuations. None of the strongly simplified models from Smith [5] or Rose

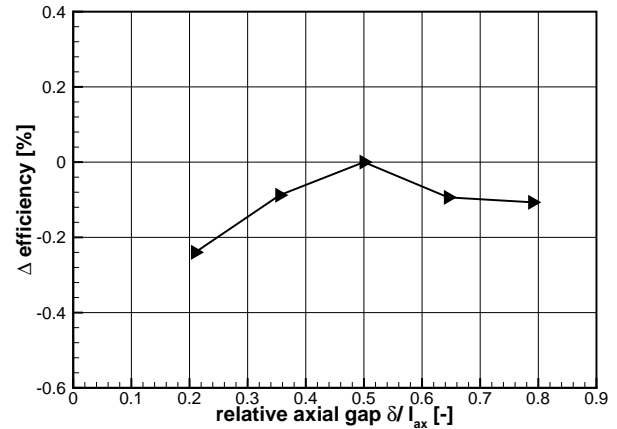


FIGURE 16: SIMULATION RESULTS FOR THE 2D CALCULATION

and Harvey [7] is solely capable of predicting the correct losses with varying inter blade row axial gaps for the two-dimensional case. This becomes even more evident in the three-dimensional case.

CONCLUSION

The effect of inter blade row gap variation has been investigated both numerically and experimentally for a specific turbine geometry. The main results are summarized below:

1. For this specific geometry the small axial gap is more efficient from the aerodynamic perspective. This is shown by steady, unsteady and experimental results.
2. The increase in efficiency is mainly attributed to the endwalls whereas in the freestream no distinct correlation could be found. This implies that a short axial gap is more beneficial for low aspect ratio turbines.
3. The flow in the second stator passage is not influenced as strongly as in the rotor passage and the results show that the secondary flows in the second stator are augmented by the small axial spacing. The upstream rotor and stator have a contradictory effect on the second vane.
4. The influence of time average negative incidence on the efficiency improvement could be shown and is in line with former studies.
5. Both experimental data and numerical computations show a reasonable agreement improving the plausibility of the results. Unsteady calculations in general provide better agreement with the experiments.

Future research activities should clarify the influence of aspect ratio, blade loading and 3D blade design on the correlations we

found and offer improved understanding of the underlying physical mechanisms. This will help the turbine designer to use this knowledge in future turbine designs with optimized blade row gaps. Although the potential of efficiency increase is relatively small for this geometry it is worth considering it throughout the design process.

ACKNOWLEDGMENT

The investigations were conducted as part of the joint research programme COORETEC-turbo in the frame of AG Turbo. The work was supported by the Bundesministerium für Wirtschaft und Technologie (BMWi) as per resolution of the German Federal Parliament under grant number 0327715I. The authors gratefully acknowledge AG Turbo and MTU Aero Engines GmbH for their support and permission to publish this paper as well as DLR Cologne for support in use of the TRACE solver. The responsibility for the content lies solely with the authors.

NOMENCLATURE

l	chord length
δ	axial gap
t	pitch
h	blade height
s	specific entropy
R	specific gas constant
T	temperature
p	pressure
N	rotor speed
D	torque
\dot{m}	massflow
κ	specific heat ratio
c_p	specific heat
Tu	turbulence intensity
ω	vorticity
f	frequency
Ω	reduced frequency
c	velocity vector
u, v, w	cartesian velocity components
x, y, z	cartesian coordinates
Ma	mach number
α	yaw angle in absolute system
γ	pitch angle

subscripts

0	inlet
4	outlet

ax	axial
sw	stream wise
red	reduced
t	total
LE1	first stator
LE2	second stator

superscripts

-	averaged quantity
---	-------------------

REFERENCES

- [1] Moczala, M., von Lavante, E., and Parvizinia, M., 2003. "Numerical investigation of losses due to unsteady effects in axial turbines". *ASME paper GT-2003-38838*.
- [2] Kelecy, F., Griffin, J., and Delaney, R., 1995. "The effect of vane-blade spacing on transonic turbine stage performance". *AGARD CP-571*.
- [3] Cho, J. J., Kim, K. S., Kim, J. H., and Jeong, E. H., 2006. "An experimental study on the flow characteristics of a supersonic turbine for the axial gap ratio". *Proceedings of the Conference on Aerospace Propulsion AJCPP2006-22083*.
- [4] Venable, B. L., Delaney, R. A., Busby, J. A., Davis, R. L., Dorney, D. J., Dunn, M. G., Haldeman, C. W., and Abhari, R. S., 1999. "Influence of vane-blade spacing on transonic turbine stage aerodynamics: Part i-time-averaged data and analysis". *Journal of Turbomachinery*, **121**, pp. 663–672.
- [5] Smith, L. H., 1966. "Wake dispersion in turbomachines". *Journal of Basic Engineering*, **88**, pp. 688–689.
- [6] Praisner, T., Clark, J., Nash, T., Rice, M., and Grover, E., 2006. "Performance impacts due to wake mixing in axial-flow turbomachinery". *ASME paper GT2006-90666*.
- [7] Rose, M. G., and Harvey, N. W., 1999. "Turbomachinery wakes: Differential work and mixing losses". *ASME paper 99-GT-25*.
- [8] Park, J., Choi, M., and Baek, J., 2003. "Effects of axial gap on unsteady flow in one-stage axial turbine". *International Journal of Turbo and Jet Engines*, **20**, pp. 315–333.
- [9] Kikuchi, M., Funazaki, K., Yamada, K., and Sato, H., 2008. "Detailed studies on aerodynamic performance and unsteady flow behaviors of a single turbine stage with variable rotor-stator axial gap". *International Journal of Gas Turbine, Propulsion and Power Systems*, **2**, pp. 30–37.
- [10] Yamada, K., Funazaki, K., M.Kikuchi, and Sato, H., 2009. "Influences of axial gap between blade rows on secondary flows and aerodynamic performance in a turbine stage". *ASME paper GT2009-59855*.
- [11] Gaetani, P., Persico, G., Dossena, V., and Osnaghi, C., 2006. "Investigation of the flow field in a hp turbine stage for two stator-rotor axial gaps: Part 2: Unsteady flow field". *ASME paper GT2006-90556*.
- [12] Gaetani, P., Persico, G., Dossena, V., and Osnaghi, C.,

2006. "Investigation of the flow field in a hp turbine stage for two stator-rotor axial gaps: Part 1 -3d time-averaged flow field". *ASME paper GT2006-90553*.
- [13] Gaetani, P., Persico, G., and Osnaghi, C., 2007. "Effects of the axial gap on the vane - rotor interaction in a hp turbine stage". *ISABE-2007-1344*.
- [14] Cizmas, P., Hoenninger, C., Chen, S., and Martin, H., 2001. "Influence of inter-row gap value on turbine losses". *International Journal of Rotating Machinery*, **7**(5), pp. 335–349.
- [15] van de Wall, A. G., Adamczyk, J. J., and Kadambi, J. R., 2000. "A transport model for the deterministic stresses associated with turbomachinery blade row interactions". *Journal of Turbomachinery*, **122**, pp. 593–603.
- [16] Gier, J. e. a., 2008. "Designing low pressure turbines for optimized airfoil lift". *ASME Turbo Expo 2008: Land, Sea and Air GT2008, Berlin, Germany*.
- [17] Halstead, D., Wisler, D., Okilshi, T., Walker, G., Hodson, H., and Shin, H.-W., 1997. "Boundary layer development in axial compressors and turbines: Part 1 of 4 - composite picture". *Journal of Turbomachinery*, **119**, pp. 114–127.
- [18] Gostelow, J. P., 1977. "A new approach to the experimental study of turbomachinery flow phenomena". *Journal of engineering for power*, **99**, pp. 97–105.
- [19] Poehler, T., Gier, J., and Jeschke, P., 2010. "Numerical and experimental analysis of the effects of non-axisymmetric contoured stator endwalls in an axial turbine". *ASME paper GT2010-23350*.
- [20] Walraevens, R., 2000. "Experimentelle analyse dreidimensionaler instationärer strömungseffekte in einer 1 1/2-stufigen axialturbine". PhD thesis, Fortschrittsberichte VDI, Reihe 7, Nr. 385, Düsseldorf, VDI-Verlag.
- [21] Nuernberger, D., and Greza, H., 2003. "Numerical investigation of unsteady transitional flows in turbomachinery components based on a rans approach". *Flow, Turbulence and Combustion*, **69**.
- [22] Kügeler, E., Weber, A., and Lisiewicz, S., 2001. "Combination of a transition model with a twoequation turbulence model and comparison with experimental results". In Proc. 4th Eu. Conf. TurbMach, ATI-CST-076/01, Florence, Italy.
- [23] Weber, A., 2004. 3d structured grids for multistage turbomachinery applications based on g3dmesh. Tech. rep., DLR-Internal Report 325-05-04.
- [24] Giles, M., 1990. "Nonreflecting boundary conditions for euler equation calculations". *AIAA Journal*, **28**, pp. 2050–2058.
- [25] Yang, H., Nuernberger, D., Nicke, E., and Weber, A., 2003. "Numerical investigation of casing treatment mechanisms with a conservative mixed-cell approach". *ASME paper GT2003-38483*.
- [26] Kozulovic, D., Roeber, T., and Nuernberger, D., 2007. "Application of a multimode transition model to turbomachinery flows". *Proc. 7th European Turbomachinery Conference, Athens (Greece)*.
- [27] Clark, J., and Grover, E., 2007. "Assessing convergence in predictions of periodic-unsteady flowfields". *Journal of Turbomachinery*, **129**, pp. 740–749.
- [28] Greitzer, E. M., 1984. Unsteady flows in turbomachines, lecture series 1984-02. Lecture series, von Karman Institute for Fluid Dynamics, Rhode-St-Genese, Belgium, February.
- [29] Horlock, J. H., and Lakshminarayana, B., 1973. "Secondary flows: Theory, experiment, and application in turbomachinery aerodynamics". *Annual Review of Fluid Mechanics*, pp. 247–280.
- [30] Persico, G., Gaetani, P., Dossena, V., D'Ippolito, G., and Osnaghi, C., 2009. "On the definition of the secondary flow in three-dimensional cascades". *Proceedings of the Institution of Mechanical Engineers, Part A: Journal of Power and Energy*, **223**, pp. 667–676.
- [31] Denton, J. D., 1993. "Loss mechanisms in turbomachines". *Journal of Turbomachinery*, **115**, pp. 621–656.
- [32] von Hoyningen-Huene, M., and Hermeler, J., 1999. "Time-resolved numerical analysis of the 2-d aerodynamics in the first stage of an industrial gas turbine for different vane-blade spacings". *ASME paper 1999-GT-102*.